A R C H I V E S O F M E T A L L U R G Y A N D M A T E R I A L S
Volume 60 2015 Issue 3
DOI: 10.1515/amm-2015-0373

M.J. SZCZERBA*#

# NON-MODULATED MARTENSITE MICROSTRUCTURE WITH INTERNAL NANOTWINS IN Ni-Mn-Ga ALLOYS

# NIE-MODULOWANA MARTENZYTYCZNA MIKROSTRUKTURA Z WEWNĘTRZNYMI NANO-BLIŹNIAKAMI W STOPACH Ni-Mn-Ga

The self-accommodated non-modulated martensite of Ni-Mn-Ga single crystal was studied by transmission and scanning electron microscopy in the latter case using the electron backscatter diffraction technique. Three kinds of interfaces existing at different length scales were reported. The first, is the wavy and incoherent interface separating martensite variants observed on the micro-level with no-common crystallographic plane between them. The second is within a single martensite plate where the lattice rotates around one of the {110} pole to accommodate the interfacial curvature between martensite plates. Finally, at the nanoscale the third interface exists, a twin boundary separating internal nanotwins with the {112} type habit plane.

*Keywords:* shape memory alloys; martensite; Ni-Mn-Ga single crystals; interface

W pracy przeprowadzono obserwacje mikrostruktury monokryształu Ni-Mn-Ga charakteryzujący się nie-modulowaną strukturą martenzytyczną. Badania przeprowadzono z wykorzystaniem techniki transmisyjnej oraz skaningowej mikroskopii elektronowej. W przypadku drugiej metody zastosowano technikę elektronów wstecznie rozproszonych. Trzy rodzaje granic zostały zaobserwowane oraz opisane. Pierwsza granica jest niekoherentna i występuje w skali mikro pomiędzy płytkami martenzytu, które nie posiadają wspólnej płaszczyzny krystalograficznej o niskich indeksach Millera. Kolejna granica występuje wewnątrz pojedynczej płytki martenzytycznej, której towarzyszy rotacja sieci krystalicznej wokół kierunku {110} obszarów przedzielonych tą granicą w celu akomodacji wygięć granicy występującej między płytkami. W skali nanometrycznej można zaobserwować kolejną granicę równoległą do płaszczyzny krystalograficznej {112} (płaszczyzna bliźniacza), która rozdziela płytki nanobliźniaków.

## 1. Introduction

It is now widely accepted that the magnetic field induced strain (MFIS) occurs in 10M and 14M modulated martensite structures of Ni-Mn-Ga single crystals [1-3]. The microstructure of modulated martensites has been thoroughly studied by x-ray and electron backscatter diffraction (EBSD) techniques revealing a more complex character of twin boundaries than earlier assumed [4-7]. The complexity of different kinds of twin boundaries (i.e. type I and type II) coupled with the a/b and modulation boundaries recently reported in [5] seem to account for different levels of critical twinning stress observed during martensite reorientation in modulated structures. On the other hand, the non-modulated (NM) structure due to the relatively high critical twinning stress and insufficient magnetic crystalline anisotropy was considered incapable of possessing the MFIS effect [8]. To date, this is the main reason why the microstructure and other related properties of NM martensite has been less frequently studied [9-11]. However, very recently giant MFIS of 12% of longitudinal strain was observed by Sozinov et al. [12] in NM Ni-Mn-Ga based single crystals opening new possibilities for Ni-Mn-Ga system as a functional material. In particular, considering significantly higher temperature of martensitic transformation observed in NM structures expanding the narrow temperature range found in 10M and 14M martensites well above room temperature, which is very important for potential applications. In this paper we study the microstructure of NM martensite of Ni-Mn-Ga single crystals at different length scales and present some morphological features as well as crystallographic orientation relationships of self-accommodated martensite variants.

* INSTITUTE OF METALLURGY AND MATERIALS SCIENCE, POLISH ACADEMY OF SCIENCES, 25 REYMONTA STR., 30-059 KRAKÓW, POLAND
# Corresponding author: m.szczerba@imim.pl

## 2. Experimantal procedures

Polycrystalline ingots of Ni-Mn-Ga alloys were prepared in an arc furnace from elements of nickel, manganese and gallium (purity: Ni-99,999%, Mn-99,98%, Ga-99,999%). From these ingots large single crystal with dimensions $10\times10\times50$ mm$^3$ were grown by a modified Bridgman method in an induction furnace at a vacuum better than $10^{-5}$ hPa. A boron nitride crucible was used since it is non-reactive to each of the elements used. From a large single crystal, a smaller sample with approximately (110) [001] orientation was excised using an electro-spark machine. For scanning electron microscopy (SEM) observations of martensite morphology the sample surface after precise mechanical polishing was etched in a solution of 25% of nitride acid and 75% of ethanol. The same solution was used for thin foil preparation for transmission electron microscopy (TEM) observations. For EBSD analysis electropolishing the sample surface with the A2 Struers reagent using relatively high voltage of 30 V was a better preparation method. In all cases of sample preparation the solutions were cooled down to –20°C. Microstructure was analyzed by Hitachi S3400 SEM equipped with an EBSD detector. The indexing of Kikuchi patterns and all other crystallographic analysis presented in this paper were carried out using the unit cell of tetragonal symmetry with the I4/mmm space group. However, for clarity in some cases the so-called cubic coordinate system was also used indicated by a lower case letter C. Thin foils for TEM (TECNAI G$^2$ F20 FEG) observations were taken parallel to one of the {001} plane of the austenite phase.

## 3. Results and discussion

Fig. 1 shows typical morphology found in a self-accommodated NM Ni-Mn-Ga martensite with sets of colonies of martensite plates laying vertically and horizontally. The thickness of individual martensite plates varies from a few to several micrometers. Thicker plates have a tendency to undergone branching creating finer microstructure. This frequently occurs in the vicinity of an interaction of differently oriented martensite plates (some examples of this effect are marked by an arrow in Fig. 1). One can also observe that the inter-plate boundary (IPB) between martensite plates (e.g. A and B on Fig. 1) is not straight having a wavy character.

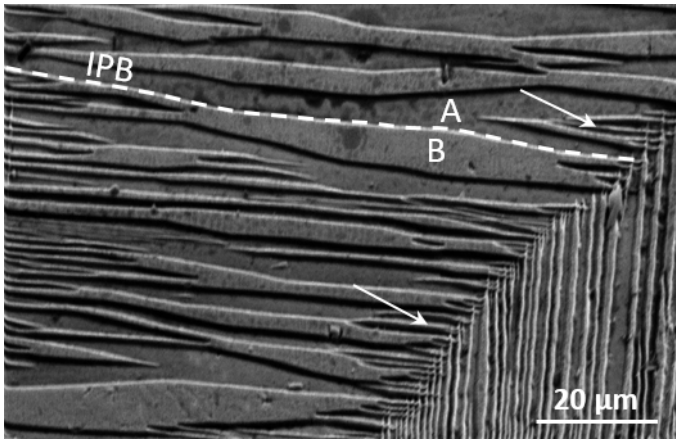


Fig. 1. SEM image of self-accommodated martensite plates of a NM Ni-Mn-Ga alloy (secondary electron mode). White dashed line shows the interface between two martensite plates denoted as A and B. Arrows indicate branching effect

Further measurements by means of EBSD technique confirm the curved character of the IPB and also show the branching effect, as can be seen in Fig. 2a.

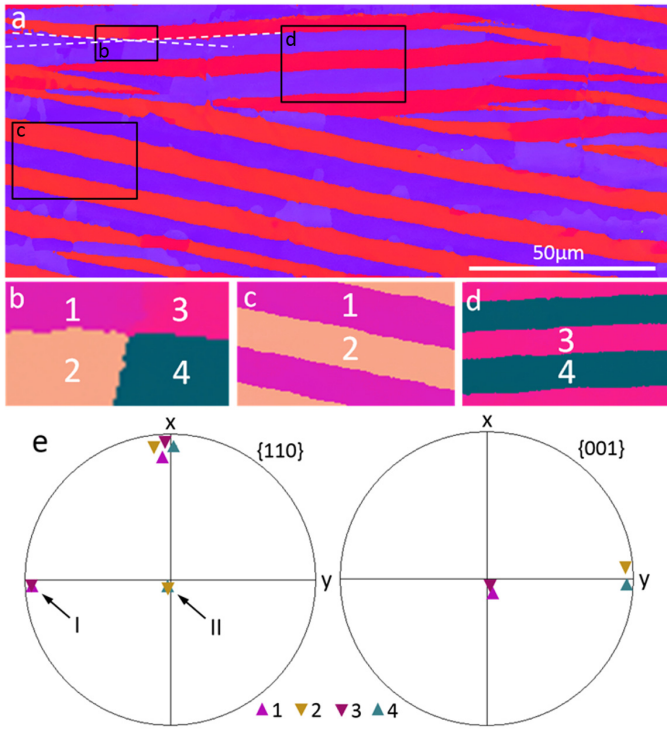


Fig. 2. EBSD image of martensite plates in Ni-Mn-Ga crystal, a). The white dashed lines are drawn to show the wavy nature of the interface. An enlarged part of the boxed regions from Fig. 2a shown in the All Euler mode in order to better visuals the small orientation differences, b, c, d) and the corresponding {110} and {001} pole figures, e)

Similar morphology was found in 10M martensite microstructure with the martensite plates separated by a curved interface and also with well-defined branching [6]. Further EBSD data analysis shows that in the vicinity of the IPB curvature, the martensite plates on both sides of the interface adjust by small lattice rotations (an example of the curvature is visualized by extrapolating from both sides the IPB by white dashed lines in Fig. 2a). In order to visualize the small orientation differences within each martensite plate and thus, the lattice rotations, an enlarged part of area b from Fig. 2a has been shown in All Euler color coding. Fig. 2b shows this area with two martensite plates in the vicinity of the curvature where four regions having different orientations were found. Regions denoted as 2 and 4 belonging to the lower martensite plate are rotated with respect to each other around the {110} pole (indexed as 1 on Fig. 2e) by ~5°. The {110} planes indexed with the unit cell having I4/mmm symmetry are physically equivalent to $\{100\}_C$ planes

in the so-called cubic coordinate system (the low C index refers to the high temperature $L2_1$ austenite phase). A similar situation concerns the upper martensite plate where the crystal lattices of regions 1 and 3 are rotated relative to each other around a different {110} pole (indexed as 2 on Fig. 2e) by a similar angle. It is to emphasized that in both cases the crystal lattices of regions 1-3 and 2-4 are rotated within the same martensite plate and the interface between those rotated regions has been recently termed conjugation boundary, CB [13]. On the other hand, when martensite plates are arranged creating lamellar structure where the interface is straight as in Figures 2c and 2d, no additional rotation within one variant is needed. As a consequence only one orientation of the crystal lattice is detected by EBSD measurements within each martensite plate and the CB in this case is not observed. In regions with a straight IPB (between 1-2 and 3-4) the lattices of martensite plates have no common low index crystallographic plane and therefore the interface separating them must be incoherent (Fig. 2e). Most importantly, the martensite plates in the lamellar structure are not twin related [14]. A consequence of this finding is that detwinning modes, responsible as has been lately shown for deformation of such a martensite structure [15,16], cannot change one martensite plate into another. Thus, deformation detwinning must take place within individual plates at a smaller length scale. The spikes between plates where the IPB is observed (see for instance Fig. 2d) are due to processing of raw data by extrapolating the boundary region usually not indexed during EBSD measurements and also to some extent because of low resolution EBSD performed in this case with a tungsten filament SEM. Therefore, these spikes must be treated as artifacts.

TEM observations of a thin foil prepared from the same sample as the above EBSD measurements indeed reveal an internal structure of martensite plates (Fig. 3a).

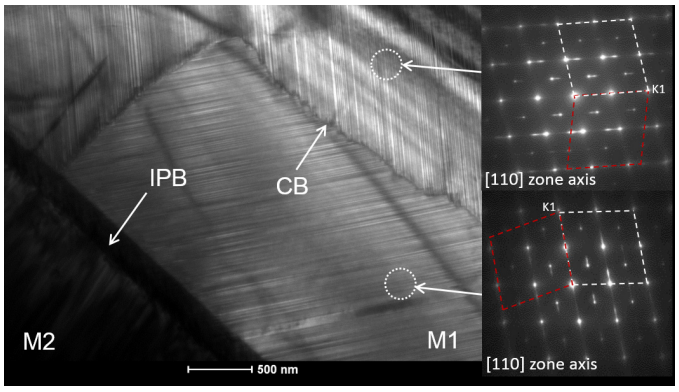


Fig. 3. TEM micrograph of two martensite plates (M1 and M2) with internal nanotwins in NM Ni-Mn-Ga crystal. Arrows indicate IPB and CB. Inserts show DP from the upper plate M2 taken with the beam parallel to [110]. The two sets of twin related lattices are marked by white and red dashed lines

The internal structure, as can be deduced from the electron diffraction pattern (DP), was composed of thin nanotwins (see insert in Fig. 3). The absence of satellite spots between the main reflections on the DP, usually seen in the case of modulated martensites, proves the existence of a non-modulated lattice of this lamellar nanotwined structure [17,18]. A large range in the thickness of nanotwins can be observed. However, the mean thickness of individual lamella measured using an intensity line profile taken across nanotwins in Fig. 4 where the twin boundary (TB) is seen edge on was about 10nm. This value is three orders of magnitude lower than the thickness of martensite plates previously identified by EBSD at a micro scale and it is below the resolutions of this technique. It is, therefore, not surprising that the internal nanotwins presented in this work and also observed in the BSE mode by Li et al. [19] could not be identified directly by SEM/EBSD measurements. The TB of nanotwins is parallel to the (112) plane which was identified as being common for both twin lattices and plays the role of the habit plane (see K1 on the insert of Fig. 3). It comes from the fact, that the K1 reflection on the DF is common for both twin lattices. Additionally, the trace of these TBs is indicated on Fig. 4 by white dashed lines. It seems that this interface is coherent, unlike the IPB separating plates M1 and M2 (Fig. 3). Within a single plate two sets of nanotwins are observed. The TBs are situated at close to 90 degrees to each other and are separated by a CB. One can observed that this boundary has a step-like character. These steps are created from conjugate twins coming from both sides of the boundary (see Fig. 4).

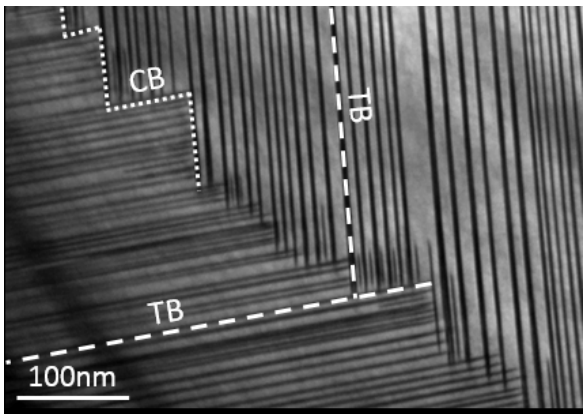


Fig. 4. TEM micrograph of a region within the vicinity of CB. Note the step-like character of CB with steps being parallel to the TB (dashed white lines) of nanotwins situated at both sides of the CB

Each step in the boundary appears to be parallel to the TB of each twin configuration. The nanotwinned structure was also observed by TEM in Ni-Mn-Ga polycrystals [9]. However, because of an unfavorable orientation of the thin foil (which was unfortunately unspecified) it was impossible to observe the step-like boundary separating different configurations of nanotwin lamellas.

Recent in-situ straining of NM Ni-Mn-Ga shows that the deformation process in Ni-Mn-Ga alloys is governed by detwinning at the nanoscale level changing one region of nanotwins into another [14-16]. The full crystallographic description of deformation detwinning in Ni-Mn-Ga single crystals performed

by means of the correspondence matrix method can be found in [20]. However, in that paper the cubic coordinate system with the $(011)_C$ being the TB was used. It must be emphasized that the above TEM observations and others found in the current literature were all performed on the as-transformed martensite microstructure of Ni-Mn-Ga alloys. However, the giant MFIS of 7%, 10% and 12% of longitudinal strain observed in 10M, 14M and NM martensites, respectively were all found in the initially trained microstructures of Ni-Mn-Ga single crystals. Training process is a sequence of uniaxial compression tests performed parallel to the $\{001\}_C$ direction referred to the cubic austenite phase [21]. The purpose of such a procedure: (i) is to lower the twinning stress in order to initiate strain by an external magnetic field and (ii) to refine the self-accommodated martensite structure achieving large MFIS determined by $c/a$ ratio where $c$ and $a$ are the unit cell parameters of a particular martensite structure. Therefore, it is important to perform TEM observations of trained Ni-Mn-Ga single crystals. Then, new questions concerning trained microstructure arise: (i) are the internal nanotwins present after performing the training process? (ii) what is the role of the step-like CB within martensite plates during training? It seems important to answer these questions especially now that the MFIS was reported in NM Ni-Mn-Ga based systems [11].

## 4. Conclusions

From detail microstructure investigation using SEM/EBSD and TEM techniques it has been shown that the NM Ni-Mn-Ga martensite is composed of martensite plates of thickness in the range of tens of micrometers separated by a curved interface (IPB) and no crystallographic plane was found common for both lattices. The curvature of the interface is accompanied by a small lattice rotation around one of the {110} poles within each martensite plate. Additionally, martensite plates are composed of an internal substructure of thin lamellas of NM nanotwins with a mean thickness of about 10nm and the {112} TB. Finally, between nanotwin configurations a CB exist having a step-like character with steps being parallel to the TB of nanotwins.

**Acknowledgements**

This work is dedicated to Prof. Bogusław Major, a former PhD advisor of M.J. Szczerba. Special thanks to Prof. W. Maziarz and Dr. R. Chulist for TEM and SEM investigations, respectively. The financial support of the National Centre of Science of Poland under Grant DEC-2011/03/D/ST8/04017 is acknowledged.

*Received: 20 April 2015*

REFERENCES

[1] S.J. Murray, M. Marioni, S.M. Allen, R.C. O'Handley, T.A. Lograsso, Appl Phys Lett **77**, 886 (2000).
[2] E. Pagounis, R. Chulist, M.J. Szczerba, M. Laufenberg, Appl Phys Lett **105**, 052405 (2014).
[3] A. Sozinov, A.A. Likhachev, N. Lanska, K. Ullakko, Appl Phys Lett **80**, 1746 (2002).
[4] O. Heczko, L. Straka L, H. Seiner, Acta Mater **61**, 622 (2013).
[5] L. Straka, O. Heczko, H. Seiner, N. Lanska, J. Drahokoupil, A. Soroka, S. Fähler, H. Hänninen, A. Sozinov, Acta Mater **59**, 7450 (2011).
[6] Z. Li, Y. Zhang, C. Esling, X. Zhang, L. Zuo, Acta Mater **59**, 3390 (2011).
[7] R. Chulist, A. Sozinov, L. Straka, N. Lanska, A. Soroka, T. Lippmann, C-G.Oertel, W. Skrotzki, J Appl Phys **112**, 063517 (2012).
[8] N. Okamoto, T. Fukuda, T. Kakeshita, T. Takeuchi, Mater Sci Eng A **438-440**, 948 (2006).
[9] M. Han, J.C. Bennett, M.A. Gharghouri, J. Chen, C.V. Hyatt, N. Mailman, Mater Charact **59**, 764 (2009).
[10] M.J. Szczerba, J. Żukrowski, M.S. Szczerba, B. Major, Arch Metall Mater **53**, 253 (2008).
[11] M.J. Szczerba, J. Przewoźnik, J. Żukrowski, Cz. Kapusta. M.S. Szczerba, B. Major, Arch Metall Mater **54**, 439 (2009).
[12] A. Sozinov, N. Lanska, A. Soroka, W. Zou, Appl Phys Lett **102**, 021902 (2013).
[13] B. Munifering, R.C. Pond, L. Kovarik, N.D. Browning, P. Müllner, Acta Mater **71**, 255 (2014).
[14] M.J. Szczerba, R. Chulist, Acta Mater **85**, 67 (2015).
[15] N. Zárubová,Y. Ge, J. Gemperlová, A. Gemperle, S.P. Hannula, Funct Mater Lett **5**, 1250006 (2012).
[16] N. Zárubová, Y. Ge, O. Heczko, S.P. Hannula, Acta Mater **61**, 5290 (2013).
[17] J. Pons, R. Santamarta, V.A. Chernenko,,E. Cesari, Mater Sci Eng A **438-440**, 931 (2006).
[18] J. Pons, R. Santamarta, V.A. Chernenko, E. Cesari, Mater Chem Phys **81**, 457 (2003).
[19] Z. Li, N. Xu, Y. Zhang, C. Esling, J.-M. Raulot, X. Zhao, L. Zuo, Acta Mater **61**, 3858 (2013).
[20] M.J. Szczerba, M.S. Szczerba, Scripta Mater **66**, 29 (2012).
[21] M.J. Szczerba, R. Chulist, S. Kopacz, M.S. Szczerba, Mat Sci and Eng. A **611**, 313 (2014).